


Article

Preparation and Catalytic Performance of Metal-Rich Pd Phosphides for the Solvent-Free Selective Hydrogenation of Chloronitrobenzene

Chunshan Lu *, Qianwen Zhu, Xuejie Zhang, Qiangqiang Liu, Juanjuan Nie, Feng Feng *, Qunfeng Zhang, Lei Ma, Wenfeng Han *  and Xiaonian Li

State Key Laboratory Breeding Base of Green Chemistry Synthesis Technology, Zhejiang University of Technology, Hangzhou 310014, China; 2111601062@zjut.edu.cn (Q.Z.); 2111701362@zjut.edu.cn (X.Z.); 2111801089@zjut.edu.cn (Q.L.); 2111801242@zjut.edu.cn (J.N.); zhangqf@zjut.edu.cn (Q.Z.); malei@zjut.edu.cn (L.M.); xnli@zjut.edu.cn (X.L.)

* Correspondence: lcszjcn@zjut.edu.cn (C.L.); ffeng@zjut.edu.cn (F.F.); hanwf@zjut.edu.cn (W.H.); Tel.: +86-571-88320836 (C.L.)

Received: 28 January 2019; Accepted: 8 February 2019; Published: 13 February 2019



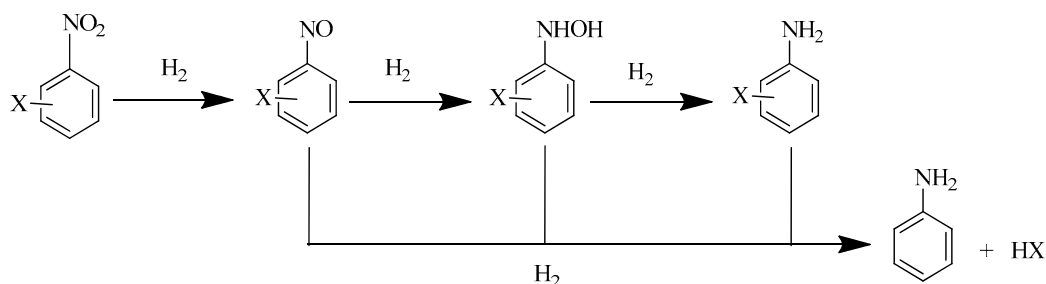
Abstract: A facile synthesis method of palladium phosphide supported on the activated carbon was developed. The effects of Pd precursors for phosphatization, phosphatization temperature, and the ratio of hypophosphite/Pd on the generation of palladium phosphide were investigated, and a generation mechanism of the Pd₃P crystal structure is proposed. The results demonstrate that only PdO, rather than Pd or PdCl₂, can transform into Pd phosphide without damage to the activated carbon. The penetration of P into the Pd particle can dramatically improve the dispersion of Pd species particles on the activated carbon. The generation of Pd phosphide greatly depends on the phosphatization temperature and the ratio of hypophosphite/Pd. An intact Pd₃P crystal structure was obtained when the ratio of hypophosphite/Pd reached 32 and the phosphatization temperature was above 400 °C. The Pd₃P supported on the activated carbon exhibited superior catalytic performance in terms of the hydrogenation of halonitrobenzenes to haloanilines because it had few L acids and B acids sites and could not generate deficient-electron active hydrogen atoms as electrophiles.

Keywords: halonitrobenzenes; palladium phosphide; Pd₃P; carbon

1. Introduction

Aromatic haloamines are widely used in the synthesis of fine chemicals including pharmaceuticals, pesticides, pigments, and liquid crystal materials [1–6]. Due to their enormous application markets, it is of great necessity to develop a convenient method to efficiently produce aromatic haloamines. It is well known that selective hydrogenation using molecular hydrogen instead of conventional chemical reducing reagents (Fe, Na₂S, etc.) is the main choice for the synthesis of aromatic haloamines because of its environmentally friendly process (Scheme 1). However, the highly selective synthesis of aromatic haloamines remains an unsolved challenge on almost all kinds of metal catalysts, such as Pt, Pd, Ni, Ru, and Au [7,8]. Numerous research efforts have been devoted to the suppression of the hydrodehalogenation side reaction, such as modulating metal particle size [9], adding organic additives [10–13], synthesizing metal complexes [14–16], adding metal promoters [7,17,18], and modifying the interaction between metal active components and metallic oxide supports [19]. Recently, co-based catalysts as representatives of non-noble metals have been proposed, and the catalytic performance of the hydrogenation of halonitrobenzenes has been explored [20]. Additionally, metal-free catalysts (such as Carbon Nanospheres [21] and Carbon Nanotubes [22]) have been

explored, and many attempts have been made. Although these catalysts exhibit excellent selectivity to haloanilines, it is far from practicable. For this reason, exploring novel environmentally friendly and efficient catalyst materials to enhance the hydrogenation of halonitrobenzenes is still strongly desired.



Scheme 1. Possible reaction pathways for the hydrogenation of halonitrobenzenes to haloanilines.

Heteroatoms-doped metal interstitial compounds have attracted considerable attention because of their technologically useful properties as catalytic materials. They have been demonstrated to improve specific catalytic performance in many reactions such as the Fischer–Tropsch reaction [23], hydrodesulfurization (HDS) [24], hydrodenitrogenation (HDN) [25], and ammonia synthesis [26,27]. Metal nitrides have also been considered great potential catalysts owing to their similarity with Group VIII metals. Recently, the temperature-programmed treatment of MoO_3 in flowing $\text{N}_2 + \text{H}_2$ has been employed to prepare β -phase molybdenum nitride ($\beta\text{-Mo}_2\text{N}$), which promotes the continuous gas phase hydrogenation of *p*-chloronitrobenzene (*p*-CNB) to *p*-chloroanilines (*p*-CAN) with 100% selectivity in terms of $-\text{NO}_2$ group reduction [16]. The ternary Pt- Mo_2N /SBA-15 catalysts have shown superior performance for the selective hydrogenation of cinnamaldehyde to cinnamyl alcohol [28]. Au/ Mo_2N as a new catalyst formulation promotes the hydrogenation of *p*-CNB with 100% selectivity to *p*-CAN. Au nanoparticles (mean size = 8 nm) enhanced hydrogen uptake with a four-fold increase in rate [29].

Transition metal phosphides, such as MoP [30,31], WP [32], Co_2P [33], and Ni_2P [34–38], are regarded as a novel type of metal-interstitial catalytic material after metal nitrides and carbides. Although the physical and chemical properties of phosphides bear a likeness to those of carbides and nitrides, they differ substantially in their crystal structure because the atomic radius of phosphorus (0.109 nm) is larger than that of carbon (0.071 nm) or nitrogen (0.065 nm) [35]. Their attractive properties encourage researchers to explore phosphorus-modified catalysts for the various catalytic reactions, including P-doped activated carbon supported Pd for the *p*-CNB hydrogenation to *p*-CAN [39], 3D Pd-P alloy networks for the formic acid electrooxidation [40], and non-metal phosphorus modified Pd/C as an oxygen reduction catalyst for direct methanol fuel cells [41]. However, study of selective hydrogenation reactions over pure palladium phosphide crystal phase is still lacking.

Herein, a facile synthesis method of palladium phosphide supported on activated carbon is developed. The effects of Pd precursors for phosphatization, phosphatization temperature, and the ratio of hypophosphite/Pd on the generation of palladium phosphide are investigated, and the generation mechanism of Pd_3P crystal structure is proposed. It was found that the penetration of P into Pd particles can dramatically improve the dispersion of Pd species particles on activated carbon and enhance selectivity to haloanilines. Pd_3P exhibited superior catalytic performance for the hydrogenation of halonitrobenzenes to haloanilines.

2. Results and Discussion

2.1. The Preparation of Palladium Phosphides Supported on Activated Carbon

The effect of addition amounts of hypophosphite ($n(\text{P})/n(\text{Pd})$) on the generation of palladium phosphides was investigated first. Figure 1 shows the X-ray diffraction (XRD) patterns of Pd-P/C catalysts treated with different addition amounts of hypophosphite. It can be seen that the deliberately

designed phosphatization precursor, PdO, was obtained by adjusting the forms of Pd ion before impregnation on the activated carbon (Figure 1g). After treatment at the temperature of 400 °C, PdO began to transform into 'Pd' gradually. Diffraction peaks at $2\theta = 39.9$, 46.5 , and 68.1° ascribed to Pd(111), Pd(200), and Pd(220) crystal facets, respectively, were found on Pd-P(0)/C(400) (Figure 1a). With the increase in addition amounts of hypophosphite, the diffraction peaks located at 39.9° became more and more dispersed (Figure 1b–e), except Pd-P(8)/C(400) (the reason will be discussed below). In fact, these peaks at 39.9° were not equal to that of the PdO/C sample because the diffraction peaks of palladium phosphides had been mixed into 'Pd' [39]. When the addition amount of hypophosphite reached up to $n(\text{P}):n(\text{Pd}) = 32$, the complete diffraction peaks of Pd₃P (PDF 03-065-2415) were clearly observed.

Further, the influence of phosphatization temperature on the generation of palladium phosphides was examined from 330 to 600 °C. As shown in Figure 2, the intact Pd₃P crystalline phase started after 400 °C. Furthermore, the clear XRD patterns (Figure 2b–d) display the same peak shape for those samples treated at above 400 °C, indicating that the particles sizes of palladium phosphides remained unchanged and that palladium phosphides nanoparticles had excellent thermal stability.

This generation process of a Pd₃P crystalline phase was further confirmed by transmission electron microscope (TEM) technology. TEM analysis of Pd-P/C catalysts treated with different addition amounts of hypophosphite was performed, and the results are shown in Figure 3. The lattice spacing distances of monometallic Pd species particles for PdO/C and Pd-P(0)/C(400) are 0.23 and 0.22 nm, corresponding to the (110) and (111) planes of PdO and Pd nanocrystals, respectively. For Pd-P(8)/C(400) and Pd-P(32)/C(400), the lattice spacing distance of Pd species particles is 0.23 nm, a feature of the Pd₃P (220) crystalline phase [42] (Figure 3e). Combining these results with the results of XRD, it is quite clear that the crystal structure of Pd species changed from PdO to Pd and then Pd₃P with the penetration of P into the Pd species lattice. In addition, the TEM images show that the particle sizes of Pd species increased first and then decreased with the increase of addition amounts of hypophosphite, consistent with the results of XRD. The mean size of the Pd species particles for Pd-P(8)/C(400) reached up to ~28.1 nm. However, this is much higher than that measured by the Scherrer formula, indicating that these particles may have formed from aggregation of the primary particles due to the introduction of a low level of P ($n(\text{P})/n(\text{Pd}) \leq 8$) into the Pd nanocrystal. Figure 4 shows a relationship diagram of the average size of Pd species particles of Pd-P/C catalysts and $n(\text{P})/n(\text{Pd})$. It very clearly exhibits the evolutionary process of the size and morphology of palladium phosphides.

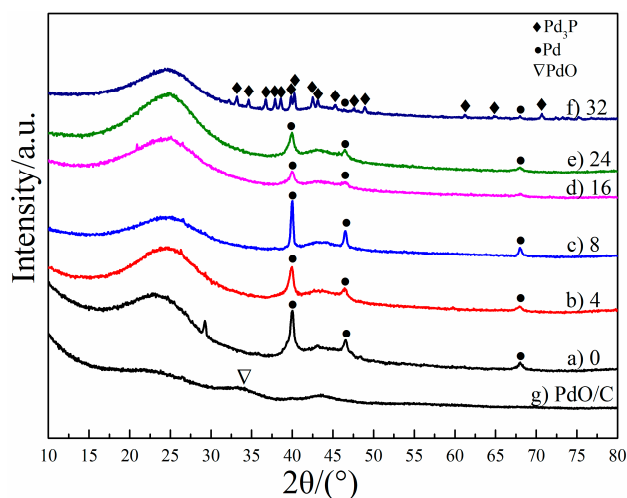


Figure 1. X-ray diffraction (XRD) patterns of Pd-P/C catalysts with different addition amounts of hypophosphite. (a) Pd-P(0)/C(400); (b) Pd-P(4)/C(400); (c) Pd-P(8)/C(400); (d) Pd-P(16)/C(400); (e) Pd-P(24)/C(400); (f) Pd-P(32)/C(400); (g) PdO/C without calcination treatment.

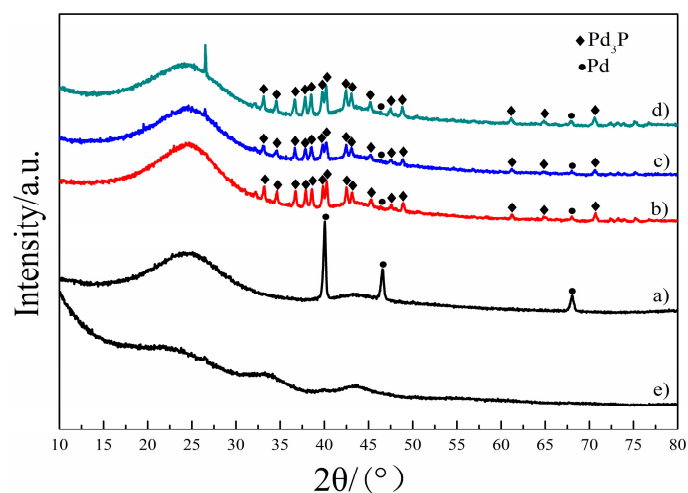


Figure 2. XRD patterns of Pd-P/C catalysts treated with different phosphating temperature. (a) Pd-P(32)/C(330); (b) Pd-P(32)/C(400); (c) Pd-P(32)/C(500); (d) Pd-P(32)/C(600); (e) PdO/C without phosphating and calcination treatment.

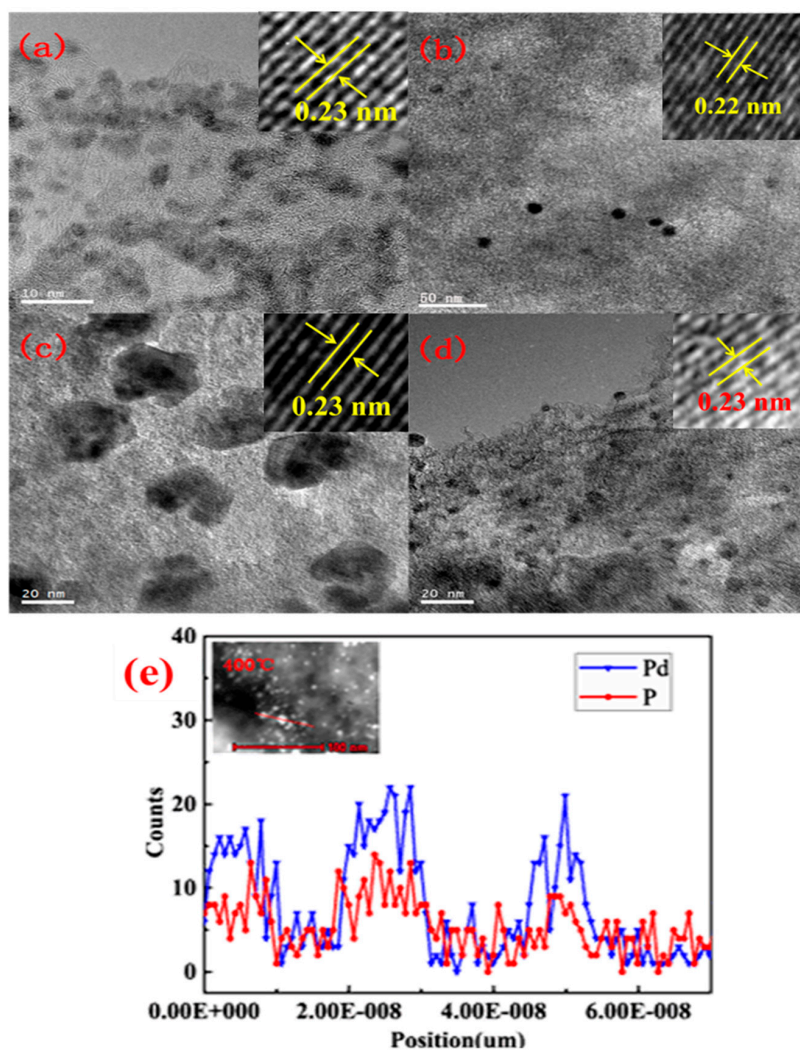


Figure 3. Transmission electron microscopy (TEM) images of Pd-P/C catalysts treated with different addition amounts of hypophosphite and PdO/C. (a) PdO/C; (b) Pd-P(0)/C(400); (c) Pd-P(8)/C(400); (d) Pd-P(32)/C(400); (e) element line scan of Pd and P of Pd-P(32)/C(400).

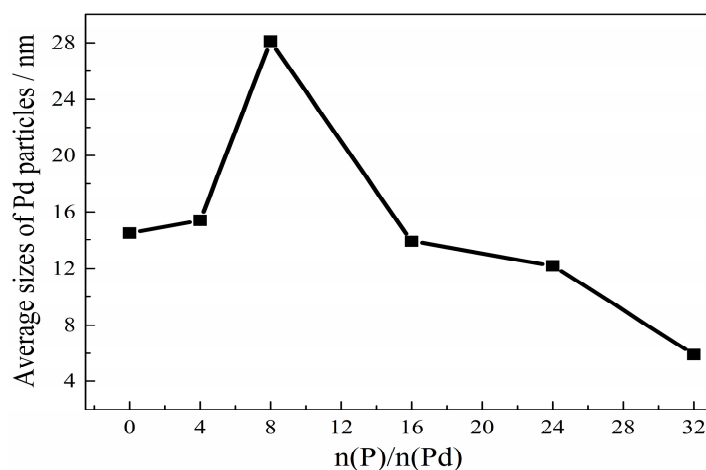


Figure 4. The relationship diagram of the average sizes of Pd particles of Pd-P/C catalysts and $n(\text{P})/n(\text{Pd})$.

For further research on the role of P in phosphatization, X-ray photoelectron spectroscopy (XPS) was employed to investigate the chemical and electronic properties of P and Pd. The Pd 3d and P 2p spectra of the samples are shown in Figures 5 and 6. The relative content and binding energy of Pd and P species are summarized in Table 1. As shown in Figure 5, the Pd 3d_{5/2} spectra present four types of peaks located at 335.60, 336.28, 337.80, and 338.40 eV, which can be assigned to Pd⁰, Pd^{x+}, Pd²⁺, and Pd⁴⁺, respectively, according to reports from Liu [43]. For PdO/C, only a Pd²⁺ peak was observed, implying that Pd species in the form of PdO exists on the catalyst without phosphatization. In contrast, Pd⁰ and Pd⁴⁺ species began to appear in Pd-P(32)/C(330) accompanied by the disappearance of PdO, suggesting that the crystal structure may have been changing dramatically. When the phosphatization temperature reached 400 °C, the Pd⁰ species completely disappeared, and Pd^{x+} became the dominant Pd species, which indicates that the transformation from PdO to Pd₃P was completed (Figures 3e and 5). Accordingly, the deconvoluted P 2p spectra demonstrate that there were two types of P species located at 130.1 eV, assigned to the P species of Pd_xP, and at 133.6–133.8 eV, ascribed to PO₄³⁻. The increase in phosphatization temperature greatly raised the content of P species but did not change the ratio of various P species (Table 1). This implies that various P species may react according to certain proportions.

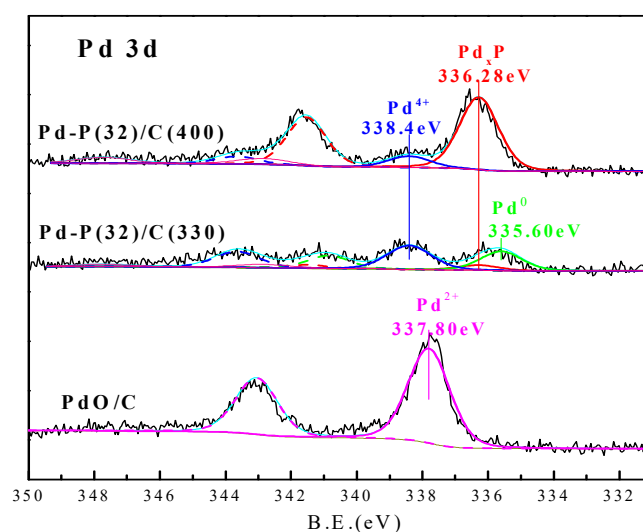


Figure 5. X-ray photoelectron spectroscopy (XPS) spectra of Pd 3d_{5/2} for PdO/C, Pd-P(32)/C(330), and Pd-P(32)/C(400).

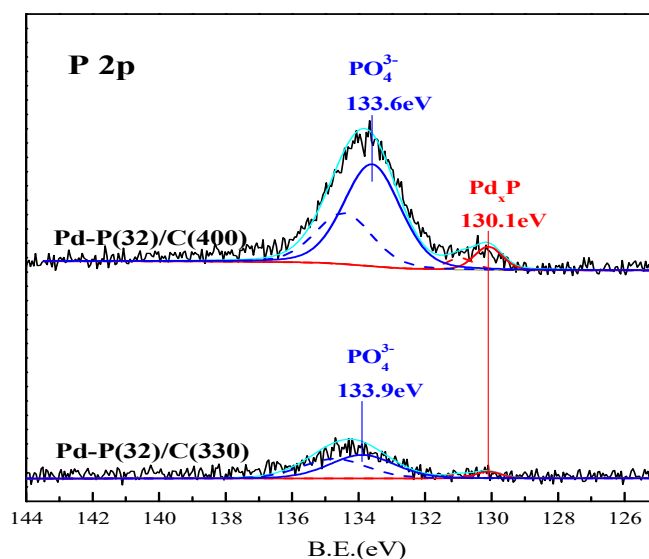


Figure 6. XPS spectra of P 2p for Pd-P(32)/C(330) and Pd-P(32)/C(400).

Table 1. Relative content and binding energy of Pd and P species of PdO/C, Pd-P(32)/C(330), and Pd-P(32)/C(400).

Catalyst	Pd Species	Pd 3d _{5/2} (eV)	Percentage (%)	P Species	P 2p _{3/2} (eV)	Percentage (%)
Pd-P(32)/C(400)	Pd _x P	336.28	85.71	Pd _x P	130.1	10.27
	Pd ⁴⁺	338.40	14.29	PO ₄ ³⁻	133.6	89.73
	Pd ⁰	335.60	38.64	/	/	/
Pd-P(32)/C(330)	Pd _x P	336.28	10.23	Pd _x P	130.1	10.20
	Pd ⁴⁺	338.40	51.13	PO ₄ ³⁻	133.9	89.80
PdO/C	Pd ²⁺	337.80	100	/	/	/

2.2. Generation Mechanism of Palladium Phosphide

Many methods or strategies have been developed to prepare metal phosphides [44–46]. However, there are relatively few studies devoted to the preparation of activated carbon-supported metal phosphides, limited by the natural properties of activated carbon. In this work, Pd and PdCl₂ supported on the activated carbon prepared with aqueous H₂PdCl₄ (Figure S1) and H₂PdCl₄ + aqua regia (Figure S2) as palladium precursors, respectively, were used to prepare Pd phosphide. The results demonstrate that only PdO can transform into Pd phosphide without damage to activated carbon. On the basis of the experiment results above, a plausible generation mechanism of palladium phosphide is proposed (Figure 7). The hydrated 'PdO' ions can be generated by adjusting the pH value of aqueous H₂PdCl₄ to 6.0–7.0 by the addition of an aqueous NaOH solution because [PdCl₄]²⁻ is easily reduced by oxygen-containing groups of activated carbon [47,48]. Thus, PdO can be kept with the activated carbon. However, a disproportionation reaction of hypophosphite will then occur and produce strong reducing PH₃ when the hypophosphite is heated. As a result, the in situ generated PH₃ will react with PdO, resulting in the replacement of the O in the PdO crystal structure with P. This replacement or penetration of P greatly depends on the ratio of hypophosphite/Pd and the phosphatization temperature.

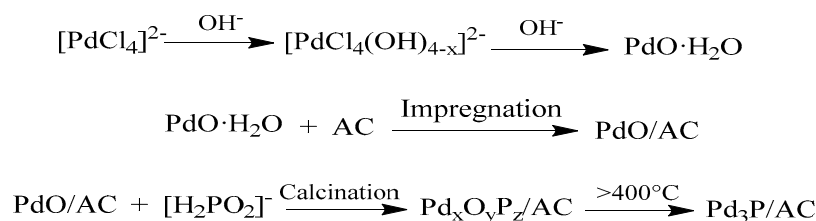


Figure 7. Generation mechanism of palladium phosphide.

2.3. Catalytic Performance of Pd₃P/AC

Solvent-free selective hydrogenation reactions of *p*-CNB to *p*-CAN were performed, and the results are listed in Table 2. As shown in Table 2, the selectivity of the dichlorination side reaction (AN, short for aniline) over Pd-P(0)/C(400) was 17.62%, similar to the general Pd/C with a similar size of Pd particle [39]. In contrast, the aniline selectivity dramatically decreased to about 2.2% when P was doped into the Pd crystal structure. XPS results show that some phosphate remained on the catalyst, so one comparable sample was prepared by supporting disodium phosphate dodecahydrate onto the fresh Pd-P(0)/C(400) catalyst according to the ratio of P-PO₄³⁻ based on the XPS result of Pd-P(32)/C(400) and was then evaluated for the hydrogenation performance of *p*-CNB. Aniline selectivity was 16.31%, indicating that the hydrodechlorination reaction was effectively suppressed due to the doping of P into the palladium catalyst. It is worth noting that Pd-P(8)/C(400) exhibited a *p*-CAN selectivity of 99.35% with a 100% conversion. However, the size of the Pd species cluster of Pd-P(8)/C(400) was so large that it could influence the selectivity of *p*-CAN [9]. Thus, it is very difficult to investigate the real role of P for the Pd phosphides. Therefore, Pd-P(32)/C(400) with an intact Pd₃P crystal phase and a particle size of 5 nm was selected as a representative for further research on the effect of P doping on Pd particles.

Table 2. Effect of phosphorus doping amounts on the selective hydrogenation of *p*-CNB under solvent-free conditions.

Catalyst	Solvents	Temperature °C	Pressure MPa	Reaction Time (min)	Conversion (%)	Selectivity (%)	
						<i>p</i> -CAN	AN
Pd-P(0)/C(400)	/	90	1.6	186	100	82.38	17.62
Pd-P(4)/C(400)	/	90	1.6	168	100	97.79	2.21
Pd-P(8)/C(400)	/	90	1.6	318	100	99.35	0.65
Pd-P(16)/C(400)	/	90	1.6	158	100	97.63	2.37
Pd-P(24)/C(400)	/	90	1.6	156	100	97.51	2.49
Pd-P(32)/C(400)	/	90	1.6	150	100	97.96	2.04
Pd-P(32)/C(400)	/	85	1.5	145	100	99.69	0.31
Pd-P(32)/C(400)	/	100	1.5	136	100	96.88	3.12
Pd-P(32)/C(400)	/	85	1.0	178	100	99.78	0.22
Pd-P(32)/C(400)	/	85	2.0	119	100	99.37	0.63
Pd-P(32)/C(400)	150 mL of methanol	85	1.5	140	100	95.12	4.82
Pd-P(0)/C(400) + Na ₃ PO ₄	/	85	1.5	267	100	83.69	16.31

Reaction conditions: *p*-CNB, 100 g; catalyst, 0.5 g; stirring rate, 1200 rpm.

Temperature and H₂ pressure have been reported to have a great influence on the selectivity for the selective hydrogenation of halonitrobenzenes [39,49]. As shown in Table 2, optimal reaction conditions were 85 °C and 1.0–1.5 MPa for Pd-P(32)/C(400) under solvent-free conditions. The selectivity to *p*-CAN reached up to 99.78%. Compared with Pd-P(8)/C(400) and Pd-P(0)/C(400), Pd-P(32)/C(400) exhibited higher selectivity to *p*-CAN, which implies that P, not the small size of Pd species, plays a crucial role in the suppression hydrodehalogenation. In addition, as shown in Table 3, Pd-P(32)/C(400) exhibited excellent catalytic performance and selectivity after six recyclings without obvious deactivation, which suggests that the Pd₃P framework structure is steady even under hydrogenation conditions.

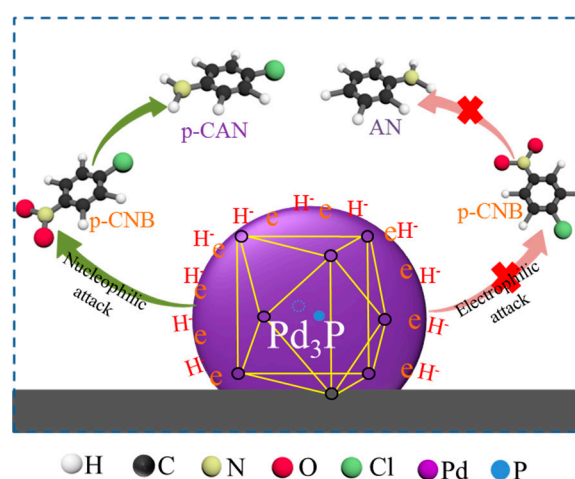
For the hydrogenation of halonitrobenzenes, the adsorption of hydrogen is involved in the rate-determining step over noble metal catalysts [50,51]. In addition, it is the dominant academic view that -NO₂ hydrogenation and C-X (X = Cl, Br, I) hydrogenolysis conform to the nucleophile and electrophilic substitution mechanism, respectively. Therefore, hydrogen species with a negative charge prefer the complete suppression of C-X hydrogenolysis. Metal phosphides have few L acids and B acids sites because of the P atom penetration into the Pd crystal structure [52,53]. This means that there are few deficient-electron sites on Pd₃P particles. As a result, Pd₃P particles are not ideal electron acceptors, and active hydrogen dissociated on Pd₃P particles has no lack of electrons, implying that such particles could not generate deficient-electron active hydrogen atoms as electrophiles. This may

be the main reason that Pd₃P supported on activated carbon exhibits superior catalytic performance in terms of the hydrogenation of halonitrobenzenes to haloanilines. A plausible catalytic mechanism of *p*-CNB hydrogenation over palladium phosphide (Pd₃P) is illustrated in Scheme 2.

Table 3. Recycling of Pd-P(32)/C(400) catalyst for selective hydrogenation of *p*-CNB under solvent-free conditions.

Recycling Time	Catalyst Addition (g)	Reaction Time (min)	Conversion (%)	Selectivity (%)	
				<i>p</i> -CAN	AN
1	0.5	148	100	99.70	0.30
2	0.025	150	100	99.66	0.34
3	0	146	100	99.68	0.32
4	0	152	100	99.70	0.30
5	0	145	100	99.71	0.29
6	0	146	100	99.69	0.31

Reaction conditions: *p*-CNB, 100 g; Pd-P(32)/C(400), 0.5 g; stirring rate, 1200 rpm; temperature, 85 °C; H₂ pressure, 1.5 MPa. Note: The catalyst was separated and recycled by the same filter paper each time.



Scheme 2. Plausible catalytic mechanism of *p*-CNB hydrogenation over palladium phosphide (Pd₃P).

3. Materials and Methods

3.1. Catalyst Preparation

PdO/C preparation: 5 g of activated carbon, made by CECA Arkema, Colombes, France (particle size: 250–300 mesh, N₂-BET: 980 m² × g⁻¹, ash content: 3%) was dried under vacuum at 110 °C for 2 h. After being cooled to room temperature, it was added to a 250 mL beaker. Subsequently, 2.0 mL of an aqueous 0.05 g_{Pd}/mL H₂PdCl₄ solution and 20 mL of deionized water were added to a 100 mL beaker under vigorous stirring at room temperature for 0.5 h. Next, the obtained aqueous H₂PdCl₄ solution was adjusted to pH 6.0–7.0 by an aqueous NaOH solution and was then added to dried activated carbon and stirred for 60 min at 30 °C. After that, the stirring was stopped and the temperature was raised to 50 °C and kept at that temperature for 4 h. The resulting product was washed with deionized water several times until the pH value was 7 and then dried at 60 °C for 12 h. The precursor was labeled PdO/C, and the nominal Pd loading was 2 wt %.

Pd-P(x)/C(t) preparation: A certain amount of sodium hypophosphite and PdO/C precursor was stirred evenly and then subjected to a temperature-programmed treatment with a heating rate of 10 °C/min under an Ar atmosphere at the desired temperature for 3 h. After slowly cooling down to room temperature, deionized water was used to completely wet the catalyst in a nitrogen atmosphere. Next, the catalyst was quickly taken out and poured into the 1% ammonia aqueous solution, stirred evenly for several minutes, and then filtered and washed with ionized water until the pH value

was 7. The black powder Pd-P(x)/C(t) was obtained where x represents the ratio of n(P)/n(Pd), and t represents the calcination temperature.

3.2. Catalyst Characterization

The X-ray diffraction (XRD) of catalysts was carried out with an X'Pert PRO diffractometer (PANalytical Co., Almelo, The Netherlands) at 45 kV and 40 mA using a Cu K α radiation source with a scanning rate of 2°/min and a step of 0.02°. TEM measurements were performed on a JEOL JEM-200CX (JEOL Ltd, Tokyo, Japan) instrument operating at 160 kV. Two hundred particles of the catalyst were randomly selected in the TEM images to calculate the mean particle size. The Brunauer–Emmett–Teller (BET) specific surface and porous parameters of the samples were measured via N₂ physical adsorption at 77 K on a Micromeritics ASAP 2020 (Micromeritics, Atlanta, GA, USA) instrument. X-ray photoelectron spectroscopy (XPS) analysis was performed on a Thermo Scientific ESCALAB 250Xi (Waltham, MA, USA). The calibration of the binding energy (BE) of the spectra was referenced to the C1s electron binding energy at 284.8 eV arising from adventitious carbon. After the linear baseline for nonmetal element signals (using the Shirley baseline for metal element signals) was subtracted, curve fitting was performed using a non-linear least-squares algorithm assuming a Gaussian peak shape.

3.3. Catalytic Hydrogenation Tests

In a typical experiment, the desired amount of *p*-CNB and catalyst were mixed together and introduced into a 700 mL stainless steel autoclave (4500 series, Parr Instrument Co., Moline, IL, USA). The reactor was sealed and purged with N₂ five times (1.0 MPa every time) and then pure H₂ five times (1.0 MPa every time) in order to replace air in the reaction system. Subsequently, the reactor was heated to the desired temperature, the H₂ gas was charged into the autoclave up to 1.0–2.0 MPa, and the stirring rate was set at 1200 r/min. During the reaction, the temperature, pressure, and stirring rate were kept constant. After the entire conversion of the halonitrobenzenes, the reactor was cooled down to room temperature, and the H₂ gas was released. The catalyst was filtered from the mixture for the next recycled use. The liquid products were qualitatively analyzed by gas chromatography (Agilent 7890, Agilent Technologies, Santa Clara, CA, USA) equipped with a programmed split/splitless inlet, a flame ionization detector (FID), and a capillary column HP-5 (30 mm \times 0.20 mm \times 0.25 μ m). The quantitative analysis of products was applied by the area normalization method.

4. Conclusions

A facile synthesis method of palladium phosphide supported on activated carbon was developed. By an investigation of the effects of Pd precursors for phosphatization, phosphatization temperature, and the ratio of hypophosphite/Pd on the generation of palladium phosphide, it was found that only PdO supported on activated carbon, rather than Pd or PdCl₂, can transform into Pd phosphide. It was found that the penetration of P into Pd particles can dramatically improve the dispersion of Pd species particles. An intact Pd₃P crystal structure was obtained when the ratio of hypophosphite/Pd reached 32 and the temperature was above 400 °C. Pd₃P particles supported on activated carbon exhibited superior catalytic performance in terms of the hydrogenation of halonitrobenzenes to haloanilines because they had few L acids and B acids sites and could not generate deficient-electron active hydrogen atoms as electrophiles.

Supplementary Materials: The following are available online at <http://www.mdpi.com/2073-4344/9/2/177/s1>, Figure S1: The XRD pattern of unreduced Pd/C, Figure S2: The XRD pattern of high dispersed PdCl₂ on Pd/C treated with aqua regia.

Author Contributions: Conceptualization, X.L. and C.L.; Methodology, C.L.; catalysts characterization, F.F.; Data curation, Q.Z.; Funding acquisition, C.L. and X.L.; Investigation, J.N. and Q.L.; Project administration, F.F. and L.M.; Resources, C.L. and X.Z.; Writing-original draft, C.L. and Q.Z.; Writing-review and editing, W.H.

Funding: Financial support by the National Natural Science Foundation of China (21406199, 21776258 and 21476208) and Program from Science and Technology Department of Zhejiang Province (LGG18B060004 and LY17B060008) are gratefully acknowledged.

Conflicts of Interest: The authors declare no conflict of interest.

References

1. Song, T.; Ren, P.; Duan, Y.N.; Wang, Z.Z.; Chen, X.F.; Yang, Y. Cobalt nanocomposites on N-doped hierarchical porous carbon for highly selective formation of anilines and imines from nitroarenes. *Green Chem.* **2018**, *20*, 4629–4637. [[CrossRef](#)]
2. Jiang, L.C.; Gu, H.Z.; Xu, X.Z.; Yan, X.H. Selective hydrogenation of o-chloronitrobenzene (o-CNB) over supported Pt and Pd catalysts obtained by laser vaporization deposition of bulk metals. *J. Mol. Catal. A Chem.* **2019**, *310*, 144–149. [[CrossRef](#)]
3. Cárdenas-Lizana, F.; Hao, Y.; Crespo-Quesada, M.; Yuranov, I.; Wang, X.; Keane, M.A.; Kiwi-Minsker, L. Selective gas phase hydrogenation of p-Chloronitrobenzene over Pd catalysts: Role of the support. *ACS Catal.* **2013**, *3*, 1386–1396. [[CrossRef](#)]
4. Zhang, Z.G.; Suo, Y.G.; He, J.P.; Li, G.N.; Hu, G.L.; Zheng, Y.Q. Selective hydrogenation of ortho-chloronitrobenzene over biosynthesized ruthenium-platinum bimetallic nanocatalysts. *Ind. Eng. Chem. Res.* **2016**, *55*, 7061–7068. [[CrossRef](#)]
5. Chen, H.; He, D.; He, Q.; Jiang, P.; Zhou, G.; Fu, W. Selective hydrogenation of p-chloronitrobenzene over an Fe promoted Pt/AC catalyst. *RSC Adv.* **2017**, *7*, 29143–29148. [[CrossRef](#)]
6. Iihama, S.; Furukawa, S.; Komatsu, T. Efficient catalytic system for chemoselective hydrogenation of halonitrobenzene to haloaniline using PtZn intermetallic compound. *ACS Catal.* **2015**, *6*, 742–746. [[CrossRef](#)]
7. Cárdenas-Lizana, F.; Gómez-Quero, S.; Hugon, A.; Delannoy, L.; Louis, C.; Keane, M.A. Pd-promoted selective gas phase hydrogenation of p-chloronitrobenzene over alumina supported Au. *J. Catal.* **2009**, *262*, 235–243. [[CrossRef](#)]
8. Ning, J.B.; Xu, J.; Liu, J.; Miao, H.; Ma, H.; Chen, C.; Li, X.Q.; Zhou, L.P.; Yu, W.Q. A remarkable promoting effect of water addition on selective hydrogenation of p-chloronitrobenzene in ethanol. *Catal. Commun.* **2007**, *8*, 1763–1766. [[CrossRef](#)]
9. Lyu, J.H.; Wang, J.G.; Lu, C.S.; Ma, L.; Zhang, Q.F.; He, X.B.; Li, X.N. Size-dependent halogenated nitrobenzene hydrogenation selectivity of Pd nanoparticles. *J. Phys. Chem. C* **2014**, *118*, 2594–2601. [[CrossRef](#)]
10. Ma, L.; Chen, S.; Lu, C.S.; Zhang, Q.F.; Li, X.N. Highly selective hydrogenation of 3,4-dichloronitrobenzene over Pd/C catalysts without inhibitors. *Catal. Today* **2011**, *173*, 62–67. [[CrossRef](#)]
11. Lu, C.S.; Lv, J.H.; Ma, L.; Zhang, Q.F.; Feng, F.; Li, X.N. Highly selective hydrogenation of halonitroaromatics to aromatic haloamines by ligand modified Ni-based catalysts. *Chin. Chem. Lett.* **2012**, *23*, 545–548. [[CrossRef](#)]
12. Mori, A.; Mizusaki, T.; Kawase, M.; Maegawa, T.; Monguchi, Y.; Takao, S.; Takagi, Y.; Sajiki, H. Novel palladium-on-carbon/diphenyl sulfide complex for chemoselective hydrogenation: Preparation, characterization, and application. *Adv. Synth. Catal.* **2008**, *350*, 406–410. [[CrossRef](#)]
13. Mori, A.; Mizusaki, T.; Miyakawa, Y.; Ohashi, E.; Haga, T.; Maegawa, T.; Monguchi, Y.; Sajiki, H. Chemoselective hydrogenation method catalyzed by Pd/C using diphenylsulfide as a reasonable catalyst poison. *Tetrahedron* **2006**, *62*, 11925–11932. [[CrossRef](#)]
14. Zhang, Q.F.; Xu, W.; Li, X.N.; Jiang, D.H.; Xiang, Y.Z.; Wang, J.G.; Cen, J.; Romano, S.; Ni, J. Catalytic hydrogenation of sulfur-containing nitrobenzene over Pd/C catalysts: In situ sulfidation of Pd/C for the preparation of Pd_xS_y catalysts. *Appl. Catal. A* **2015**, *497*, 17–21. [[CrossRef](#)]
15. Bachiller-Baeza, B.; Iglesias-Juez, A.; Castillejos-López, E.; Guerrero-Ruiz, A.; Michiel, M.D.; Fernández-García, M.; Rodríguez-Ramos, I. Detecting the genesis of a high-performance carbon-supported Pd sulfide nanophase and its evolution in the hydrogenation of butadiene. *ACS Catal.* **2015**, *5*, 5235–5241. [[CrossRef](#)]
16. Cárdenas-Lizana, F.; Gómez-Quero, S.; Perret, N.; Kiwi-Minsker, L.; Keane, M.A. β -Molybdenum nitride: Synthesis mechanism and catalytic response in the gas phase hydrogenation of p-chloronitrobenzene. *Catal. Sci. Technol.* **2011**, *1*, 794. [[CrossRef](#)]
17. Xu, X.S.; Li, X.Q.; Gu, H.Z.; Huang, Z.B.; Yan, X.H. A highly active and chemoselective assembled Pt/C(Fe) catalyst for hydrogenation of o-chloronitrobenzene. *Appl. Catal. A* **2012**, *429–430*, 17–23. [[CrossRef](#)]

18. Cárdenas-Lizana, F.; Gómez-Quero, S.; Amorim, C.; Keane, M.A. Gas phase hydrogenation of p-chloronitrobenzene over Pd–Ni/Al₂O₃. *Appl. Catal. A* **2014**, *473*, 41–50. [[CrossRef](#)]
19. Shi, W.; Zhang, B.S.; Lin, Y.M.; Wang, Q.; Zhang, Q.; Su, D.S. Enhanced chemoselective hydrogenation through tuning the interaction between Pt nanoparticles and carbon supports: Insights from identical location transmission electron microscopy and X-ray photoelectron spectroscopy. *ACS Catal.* **2016**, *6*, 7844–7854. [[CrossRef](#)]
20. Wang, X.; Li, Y.W. Chemoselective hydrogenation of functionalized nitroarenes using MOF-derived co-based catalysts. *J. Mol. Catal. A Chem.* **2016**, *420*, 56–65. [[CrossRef](#)]
21. Zhang, P.; Song, X.D.; Yu, C.; Gui, J.Z.; Qiu, J.S. Biomass-derived carbon nanospheres with turbostratic structure as metal-free catalysts for selective hydrogenation of o-chloronitrobenzene. *ACS Sustain. Chem. Eng.* **2018**, *5*, 7481–8485. [[CrossRef](#)]
22. Sergio, N.; Amarajothi, D.; Mercedes, A.; Hermenegildo, G. Carbocatalysis by graphene-based materials. *Chem. Rev.* **2014**, *12*, 6179–6212.
23. Park, B.J.; Jang, S.; Lee, J.H.; Chun, D.H.; Park, J.C.; Park, H.S. Hyperactive iron carbide@N-doped reduced graphene oxide/carbon nanotube hybrid architecture for rapid CO hydrogenation. *J. Mater. Chem. A* **2018**, *6*, 11134–11139. [[CrossRef](#)]
24. Bodin, A.; Christoffersen, A.N.; Elkjaer, C.F.; Brorson, M.; Kibsgaard, J.; Helveg, S.; Chorkendorff, I. Engineering Ni–Mo–S nanoparticles for hydrodesulfurization. *Nano Lett.* **2018**, *18*, 3454–3460. [[CrossRef](#)] [[PubMed](#)]
25. Tian, S.; Li, X.; Wang, A.J.; Chen, Y.Y.; Li, H.T.; Hu, Y.K. Hydrodenitrogenation of quinoline and decahydroquinoline over a surface nickel phosphosulfide phase. *Catal. Lett.* **2018**, *148*, 1579–1588. [[CrossRef](#)]
26. Kojima, R.; Aika, K.I. Molybdenum nitride and carbide catalysts for ammonia synthesis. *Appl. Catal. A* **2001**, *219*, 141–147. [[CrossRef](#)]
27. Zhao, J.; Zhao, J.; Cai, Q. Single transition metal atom embedded into a MoS₂ nanosheet as a promising catalyst for electrochemical ammonia synthesis. *Phys. Chem. Chem. Phys.* **2018**, *20*, 9248–9255. [[CrossRef](#)] [[PubMed](#)]
28. Wang, D.; Zhu, Y.J.; Tian, C.G.; Wang, L.; Zhou, W.; Dong, Y.L.; Han, Q.; Liu, Y.F.; Yuan, F.L.; Fu, H.G. Synergistic effect of Mo₂N and Pt for promoted selective hydrogenation of cinnamaldehyde over Pt–Mo₂N/SBA-15. *Catal. Sci. Technol.* **2016**, *6*, 2403–2412. [[CrossRef](#)]
29. Cárdenas-Lizana, F.; Lamey, D.; Perret, N.; Gómez-Quero, S.; Kiwi-Minsker, L.; Keane, M.A. Au/Mo₂N as a new catalyst formulation for the hydrogenation of p-chloronitrobenzene in both liquid and gas phases. *Catal. Commun.* **2012**, *21*, 46–51. [[CrossRef](#)]
30. Clark, P.; Wang, X.; Oyama, S.T. Characterization of silica-supported molybdenum and tungsten phosphide hydroprocessing catalysts by ³¹P nuclear magnetic resonance spectroscopy. *J. Catal.* **2002**, *207*, 256–265. [[CrossRef](#)]
31. Yang, P.F.; Jiang, Z.X.; Ying, P.L.; Li, C. Effect of surface composition on the catalytic performance of molybdenum phosphide catalysts in the hydrogenation of acetonitrile. *J. Catal.* **2008**, *253*, 66–73. [[CrossRef](#)]
32. Clark, P.; Li, W.; Oyama, S.T. Synthesis and activity of a new catalyst for hydroprocessing: Tungsten phosphide. *J. Catal.* **2001**, *200*, 140–147. [[CrossRef](#)]
33. Ni, Y.H.; Li, J.; Zhang, L.; Yang, S.; Wei, X.W. Urchin-like Co₂P nanocrystals: Synthesis, characterization, influencing factors and photocatalytic degradation property. *Mater. Res. Bull.* **2009**, *44*, 1166–1172. [[CrossRef](#)]
34. Bui, P.; Cecilia, J.A.; Oyama, S.T.; Takagaki, A.; Infantes-Molina, A.; Zhao, H.; Li, D.; Rodríguez-Castellón, E.; Jiménez López, A. Studies of the synthesis of transition metal phosphides and their activity in the hydrodeoxygenation of a biofuel model compound. *J. Catal.* **2012**, *294*, 184–198. [[CrossRef](#)]
35. Oyama, S.T.; Gott, T.; Zhao, H.Y.; Lee, Y.K. Transition metal phosphide hydroprocessing catalysts: A review. *Catal. Today* **2009**, *143*, 94–107. [[CrossRef](#)]
36. Liu, K.; Wang, Y.; Chen, P.; Zhong, W.B.; Liu, Q.Z.; Li, M.F.; Wang, Y.D.; Wang, W.W.; Lu, Z.T.; Wang, D. Noncrystalline nickel phosphide decorated poly(vinyl alcohol-co-ethylene) nanofibrous membrane for catalytic hydrogenation of p-nitrophenol. *Appl. Catal. B* **2016**, *196*, 223–231. [[CrossRef](#)]
37. Xin, H.; Guo, K.; Li, D.; Yang, H.Q.; Hu, C.W. Production of high-grade diesel from palmitic acid over activated carbon-supported nickel phosphide catalysts. *Appl. Catal. B* **2016**, *187*, 375–385. [[CrossRef](#)]

38. Cecilia, J.A.; Jiménez-Morales, I.; Infantes-Molina, A.; Rodríguez-Castellón, E.; Jiménez-López, A. Influence of the silica support on the activity of Ni and Ni₂P based catalysts in the hydrodechlorination of chlorobenzene. Study of factors governing catalyst deactivation. *J. Mol. Catal. A Chem.* **2013**, *368–369*, 78–87. [[CrossRef](#)]
39. Lu, C.S.; Wang, M.J.; Feng, Z.L.; Qi, Y.N.; Feng, F.; Ma, L.; Zhang, Q.F.; Li, X.N. A phosphorus–carbon framework over activated carbon supported palladium nanoparticles for the chemoselective hydrogenation of para-chloronitrobenzene. *Catal. Sci. Technol.* **2017**, *7*, 1581–1589. [[CrossRef](#)]
40. Zhang, J.F.; Xu, Y.; Zhang, B. Facile synthesis of 3D Pd-P nanoparticle networks with enhanced electrocatalytic performance towards formic acid electrooxidation. *Chem. Commun.* **2014**, *50*, 13451–13453. [[CrossRef](#)]
41. Cheng, L.F.; Zhang, Z.H.; Niu, W.X.; Xu, G.B.; Zhu, L.D. Carbon-supported Pd nanocatalyst modified by non-metal phosphorus for the oxygen reduction reaction. *J. Power Sources* **2008**, *182*, 91–94. [[CrossRef](#)]
42. Habas, S.E.; Baddour, F.G.; Ruddy, D.A.; Nash, C.P.; Wang, J.; Pan, M.; Hensley, J.E.; Schaidle, J.A. A facile molecular precursor route to metal phosphide nanoparticles and their evaluation as hydrodeoxygenation catalysts. *Chem. Mater.* **2015**, *27*, 7580–7592. [[CrossRef](#)]
43. Liu, Y.N.; McCue, A.J.; Miao, C.L.; Feng, J.T.; Li, D.Q.; Anderson, J.A. Palladium phosphide nanoparticles as highly selective catalysts for the selective hydrogenation of acetylene. *J. Catal.* **2018**, *364*, 406–414. [[CrossRef](#)]
44. Zhang, L.L.; Tang, Y.W.; Bao, J.C.; Lu, T.H.; Li, C. A carbon-supported Pd-P catalyst as the anodic catalyst in a direct formic acid fuel cell. *J. Power Sources* **2006**, *162*, 177–179. [[CrossRef](#)]
45. Yang, G.X.; Chen, Y.; Zhou, Y.M.; Tang, Y.W.; Lu, T.H. Preparation of carbon supported Pd–P catalyst with high content of element phosphorus and its electrocatalytic performance for formic acid oxidation. *Electrochem. Commun.* **2010**, *12*, 492–495. [[CrossRef](#)]
46. Belykh, L.B.; Skripov, N.I.; Stepanova, T.P.; Akimov, V.V.; Tauson, V.L.; Schmidt, F.K. The catalytic properties of Pd nanoparticles modified by phosphorus in liquid-phase hydrogenation of o-chloronitrobenzene. *Curr. Nanosci.* **2015**, *11*, 175–185. [[CrossRef](#)]
47. Yao, N.; Chen, J.X.; Zhang, J.X.; Zhang, J.Y. Influence of support calcination temperature on properties of Ni/TiO₂ for catalytic hydrogenation of o-chloronitrobenzene to o-chloroaniline. *Catal. Commun.* **2008**, *9*, 1510–1516. [[CrossRef](#)]
48. Bertero, N.M.; Trasarti, A.F.; Apesteguía, C.R.; Marchi, A.J. Solvent effect in the liquid-phase hydrogenation of acetophenone over Ni/SiO₂: A comprehensive study of the phenomenon. *Appl. Catal. A* **2011**, *394*, 228–238. [[CrossRef](#)]
49. Han, X.X.; Zhou, R.X.; Lai, G.H.; Zheng, X.M. Influence of support and transition metal (Cr, Mn, Fe, Co, Ni and Cu) on the hydrogenation of p-chloronitrobenzene over supported platinum catalysts. *Catal. Today* **2004**, *93–95*, 433–437. [[CrossRef](#)]
50. Vishwanathan, V.; Jayasri, V.; Basha, P.M. Vapor phase hydrogenation of o-chloronitrobenzene (o-CNB) over alumina supported palladium catalyst—A kinetic study. *React. Kinet. Catal. Lett.* **2007**, *91*, 291–298. [[CrossRef](#)]
51. Tamura, M.; Tokonami, K.; Nakagawa, Y.; Tomishige, K. Selective hydrogenation of crotonaldehyde to crotyl alcohol over metal oxide modified Ir catalysts and mechanistic insight. *ACS Catal.* **2016**, *6*, 3600–3609. [[CrossRef](#)]
52. Busca, G. Spectroscopic characterization of the acid properties of metal oxide catalysts. *Catal. Today* **1998**, *41*, 191–206. [[CrossRef](#)]
53. Devassy, B.M.; Lefebvre, F.; Halligudi, S.B. Zirconia-supported 12-tungstophosphoric acid as a solid catalyst for the synthesis of linear alkyl benzenes. *J. Catal.* **2005**, *231*, 1–10. [[CrossRef](#)]

